Accepted Manuscript

Title: Phosphonic acid functionalization of nanostructured Ni-W coatings on steel

Authors: P.A. Orrillo, S.B. Ribotta, L.M. Gassa, G. Benítez, R.C. Salvarezza, M.E. Vela

PII: S0169-4332(17)32870-2
DOI: https://doi.org/10.1016/j.apsusc.2017.09.222
Reference: APSUSC 37301

To appear in: *APSUSC*

Received date: 17-6-2017
Revised date: 8-9-2017
Accepted date: 26-9-2017

Please cite this article as: P.A.Orrillo, S.B.Ribotta, L.M.Gassa, G.Benítez, R.C.Salvarezza, M.E.Vela, Phosphonic acid functionalization of nanostructured Ni-W coatings on steel, Applied Surface Science https://doi.org/10.1016/j.apsusc.2017.09.222

Phosphonic acid functionalization of nanostructured Ni-W coatings on steel

P. A. Orrillo[1], S.B.Ribotta[1], L.M. Gassa[2], G.Benítez[2], R.C.Salvarezza[2], M.E.Vela*[,2]

[1] INQUINOA-CONICET, Instituto de Química Física, Facultad de Bioquímica, Química y Farmacia, Universidad Nacional de Tucumán, Ayacucho 471, (4000) San Miguel de Tucumán, Argentina.

[2] Instituto de Investigaciones Fisicoquímicas Teóricas y Aplicadas (INIFTA), Universidad Nacional de La Plata - CONICET- Sucursal 4 Casilla de Correo 16, (1900) La Plata, Argentina

*Corresponding author:

María Elena Vela

Address: INIFTA. Diagonal 113 esquina 64. CC 16 Suc 4 (1900) La Plata. ARGENTINA. TE +54 221 4257430, FAX: +54 221 4254642

E-mail: mevela@inifta.unlp.edu.ar

Highlights

- Robust and stable octadecylphosphonic acid self-assembled layers on nanostructured Ni-W coatings on steel were obtained by thermal annealing.
- XPS, Raman, contact angle and electrochemical measurements confirm the functionalization and characteristics of the phosphonic layer.
- The functionalized Ni-W samples exhibit high hydrophobicity and corrosion resistance in chloride containing solutions

Abstract

The functionalization of nanocrystalline Ni-W coatings, formed by galvanostatic pulsed electrodeposition on steel, by thermal treatment of octadecylphosphonic acid self-assembled on the oxidized alloy surface is studied by Raman spectroscopy, contact angle measurements, X-ray photoelectron spectroscopy, AFM and electrochemical techniques. Results show that this procedure preserves the surface topography and the optimum mechanical properties of the alloy. More importantly, it turns the alloy surface highly hydrophobic and markedly improves its corrosion resistance, in particular to pitting corrosion in aggressive solutions containing chloride anions. The ability of the phosphonate layer to improve surface properties arises from the barrier properties introduced by the hydrocarbon chains and the strong bonds between the phosphonate head and the underlying surface oxides.

Keywords: phosphonic acids, Ni W alloys, nanostructured materials, surface functionalization.

Introduction

The electrodeposition of adherent nanocrystalline Ni–W coatings on carbon steel constitutes a versatile method to improve its hardness and corrosion resistance. The composition and grain size of the Ni-W surface layer can be controlled thorough the composition of the electrolytic bath, pH, temperature and the parameters of the electrodeposition method. [1-12]

In order to further improve the corrosion protection and/or eventually perform the postfunctionalization of the surface for specific applications of the Ni/W coated steel substrates, the use of organic coatings appears as a suitable and simple procedure. [13, 14] The protective properties of these coatings are mainly determined by the strength of the bond between the metal and the organic molecules and also by the magnitude of their intermolecular interactions, both factors controlling their stability in a given environment. Silanes or phosphonates have been used for metal surfaces that are covered by their oxides.[15] Silane chemistry offers many alternatives to surface functionalization but in many cases, the poor hydrolytic stability of the siloxanes and polymerization reactions limit a precise control of the composition and structure of the layer. [16-19] Phosphonic acids ($R\text{-}PO_3H_2$) have a reactive head that forms robust and stable P-O-metal bonds and an organic tail that confers a high degree of order to these 2D or 3D metal organic frameworks.[15, 20] The P-O-metal bond can vary from ionic to covalent as a function of the identity and oxidation state of the metal ion. They have been studied on oxidized metallic surfaces and alloys such as Al[21-26], Hf[27], Nb[21, 28], Ti[29-34], In[35], In-Zn[36], Zr[37, 38], Ta[39], Mg[40, 41], Ti-Nb[42], Ni[43], Ni-Ti[44, 45], Cu[46], Ni-Cu[47], Co-Cr alloys[48], Zn[49], Fe[49] and stainless steel[50-54]; and also on Si[55, 56] , iron oxide nanoparticles[57] and ITO films[58].

When alkanephosphonic acids assembled from solution are gently heated on the native oxide surface, they form alkane chain ordered films that strongly bind to the surface and resist solvent washing or simple mechanical peel testing.[29, 59] These properties make phosphonate platforms very promising candidates for real life applications that require long-term stability of the deposited monolayer. Furthermore, interfacial properties can be controlled according to the chemical nature of the phosphonate tail by improving certain qualities of the underlying substrate, properly designing a supramolecular platform or fulfilling biocompatibility requirements.[59]

In this work we show that nanocrystalline Ni–W alloy coatings on steel can be functionalized by thermal treatment of octadecylphosphonic acid self-assembled on the oxidized surface. This procedure preserves the surface topography and the optimum mechanical properties of the alloy. The characterization of the functionalized surface was performed by X-ray photoelectron spectroscopy (XPS), atomic force microscopy (AFM), Raman spectroscopy, contact angle, cyclic voltammetry and electrochemical impedance spectroscopy (EIS). The ability of the phosphonate layer to improve the protective properties against corrosion in chloride-containing solution compared with the bare Ni-W surface evidences the combination of the barrier properties of the alkane moiety and the strength of the phosphonate head with the underlying Ni-W substrate.

Experimental

Nanocrystalline Ni–W coatings were deposited on carbon steel (SAE 1020) sheets (area = 1 cm^2) that were previously polished with grit paper in decreasing size from 180 to 2500 followed by 0.3 μm alumina powder. Finally, they were rinsed with twice-distilled water.

The electrodeposited coatings were obtained galvanostatically by pulse electroplating using an galvanostat-potentiostat TEQ 4, NanoTeq. The pulse scheme consisted of an "on" time (τ_{on}), during which a cathodic current of 140 mA cm^{-2} was applied, and an "off" time (τ_{off}), during

which a zero current was applied, where $\tau = \tau_{on} = \tau_{off} = 5$ ms. The deposition time (t_{dep}) was 60 min.[10]

The plating bath contained 0.06 M $NiSO_4.6H_2O$, 0.14 M $Na_2WO_4.2H_2O$, 0.5 M $Na_3C_6H_5O_7.2H_2O$, 0.5 M NH_4Cl, and 0.15 M NaBr (pH = 9.5). A fresh plating bath was prepared for each experiment using pure chemical reagents and deionized H_2O (18 MOhm cm) from a Milli-Q purification system (Millipore Products, Bedford). This electrodeposition solution produces amorphous and nanocrystalline Ni–W with high hardness.[10] The solution was gently stirred during the plating at 65 ºC and degassed with purified nitrogen.

Freshly prepared Ni-W steel electrodes were placed in 10^{-3} M octadecylphosphonic acid (ODPA) solutions in tetrahydrofuran (THF) for 1 h. They were then subjected to heat annealing in an oven at 100 ºC for 2 h. Finally, they were rinsed and sonicated in THF to obtain functionalized Ni-W coatings, hereafter called Ni-W&ODPA. The surface composition was evaluated by XPS using an Al Kα source (1486.6 eV) XR50, SPECS GmbH, and a hemispherical electron energy analyzer PHOIBOS 100, SPECS GmbH operating at 40 eV pass energy. A two-point calibration of the energy scale was performed using sputtered gold and copper samples (Au 4f 7/2 binding energy(BE) = 84.00 eV; Cu 2p 3/2 BE = 932.67 eV). C 1s at 285 eV was used as charging reference. Spectra fitting were performed with XPSPeak 4.1 software using a Shirley type baseline and a product of Gaussian and Lorentzian functions for the peaks. Quantitative analysis was performed taking into account the Scoffield cross sections for each element.

Static contact angle (CA) characterizations were carried out with a ramé-Hart goniometer (model 500, Netcong, NJ) with water as the probe liquid. Measurements were performed on at least three different points to calculate the average static CA. Raman spectra were obtained on a DXR Thermo Scientific Raman Microscope. A diode-pumped solid state (DPSS) laser at 532 nm with 10 mW power was used as the excitation source for the Raman experiment. A long-working-

length 10X objective was used to focus the laser spot onto the electrode surface. The pinhole was set at 50 μm. Each spectrum was measured 200 times to improve the signal to noise ratio and thus detecting more precisely the significant peaks. The acquisition time was 4 s. Raman spectra were acquired in the 900-1400 cm^{-1} and 1700-2200 cm^{-1} regions where information about the phosphate group and of methylene and methyl groups respectively can be obtained.

Surface topography was imaged with tapping AFM under ambient conditions using a MultiMode Scanning Probe Microscope (Veeco, Santa Barbara, CA, USA) equipped with a Nanoscope V controller. All the measurements were performed using sharpened silicon probes (nominal force constant of 40 N/m from Bruker) with nominal tip radius of 8 nm.

Microhardness measurements were carried out with a FUTURE-TECH microindenter. The measurements were performed on samples cross-sections applying a load of 10 g for 10 s.

To evaluate the corrosion resistance of the Ni–W coatings with and without the phosphonate layer, a single triangular potential sweep (STPS) between preset cathodic and anodic switching potentials, at a potential scan rate (v) in the 0.002 V $s^{-1} \leq v \leq$ 0.020 V s^{-1} range, and polarization curves obtained at a low scan rate (0.002 V s^{-1}) were applied in a still phosphate–borate buffer (0.1 M KH_2PO_4 + 0.05 M $Na_2B_4O_7$) pH 8.00, with the addition of 0.5 M NaCl to the same solution. A standard three–electrode cell with a large area Pt sheet counter electrode and a saturated calomel reference electrode (SCE) were used. All potentials in the text were referred to the SCE (0.241 V vs SHE). Experiments were done under purified N_2 gas saturation at 25 °C. EIS measurements were carried out at open circuit potential (OCP) by imposing a small amplitude sinusoidal perturbation (5 mV peak-to-peak) in the frequency range 30 kHz $\geq f \geq$ 10 mHz, with $f = \omega/2\pi$ using a Zahner IM6e. Data were processed using an algorithm that minimizes the error by nonlinear least squares (CNLS, Complex Nonlinear Least Squares).

Results and Discussion

The spectra of ODPA powder, bare Ni-W and Ni-W&ODPA samples are shown in Figure 1. The rinsed Ni-W&ODPA sample exhibits almost the same spectral features as the ODPA powder, although the bands in the low frequency range are barely visible. ODPA powder sample shows bands at 950, 1062, 1103, 1130, and 1296 cm^{-1}. Peaks at 900–950 cm^{-1} are assigned to P–O–H stretches. [47, 53] Peaks in the 1000–1150 cm^{-1} range can be assigned to P-O stretches [52] and the band at 1296 cm^{-1} should correspond to the CH_2 twist mode. [60-62] In the high frequency range ODPA powder exhibits bands at 2846, 2880, 2906, and 2933 cm^{-1} that could be assigned to the vibrational C-H modes of methylene groups.[63-65]. A much less intensity shoulder in the 2960-2966 cm^{-1} range could be assigned to antisymmetric methyl stretching vibrations. [63, 66] We also recorded Raman spectra for the rinsed samples, but after the sonication procedure. In this case the band intensities are too low to identify the different ODPA contributions present in the surface layer. This fact strongly suggests that ODPA multilayers have been removed by sonication, leaving a thinner layer whose composition will be explored by XPS. In fact, surface analysis by XPS allows for the qualitative and quantitative determination of the uppermost layers elements of material surfaces and their oxidation states helping, in our case, to establish the nature the phosphonate adsorption on the Ni-W coatings.

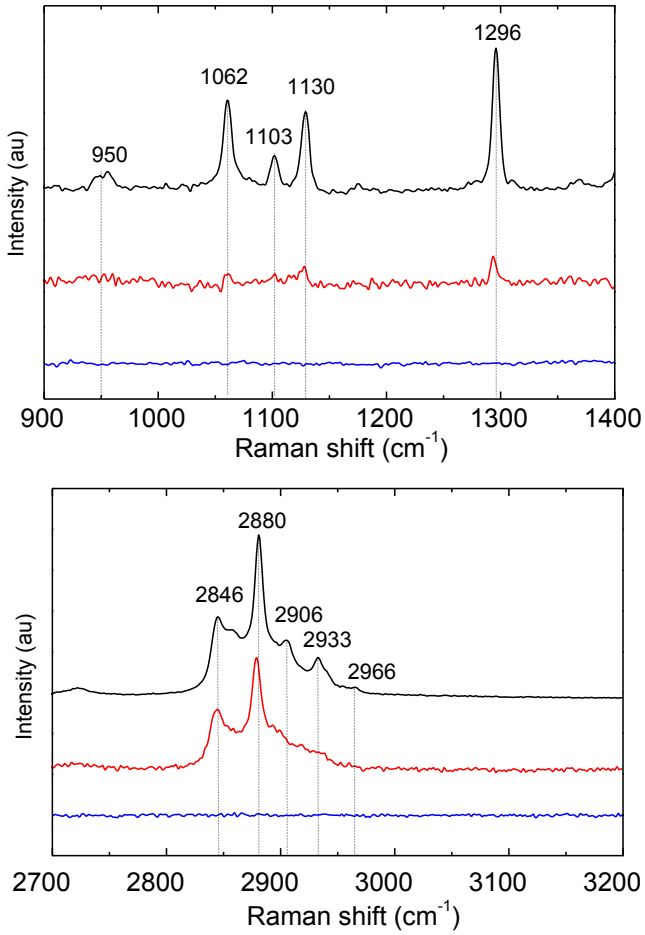

Figure 1. *Raman spectra of ODPA powder (black), Ni-W&ODPA rinsed with THF (red) and Ni-W without functionalization (blue).*

In Figure 2 low resolution spectra of bare Ni-W (Figure 2a) and the Ni-W&ODPA after sonication (Figure 2b) are displayed. In both samples, the survey scans exhibit the photoelectric and Auger lines for O, W, C, Ni, and also the P signal in the ODPA functionalized samples. The C signal is also evident not only in the Ni-W&ODPA due to the presence of the hydrocarbon chains [26] but also in Ni-W sample due to the adsorption of citrate anions, a component of the plating bath, on the oxide layer.[67] It should be pointed out that Fe is not present in these

spectra, indicating that the bare and functionalized Ni–W coating entirely covers the underlying steel substrate.

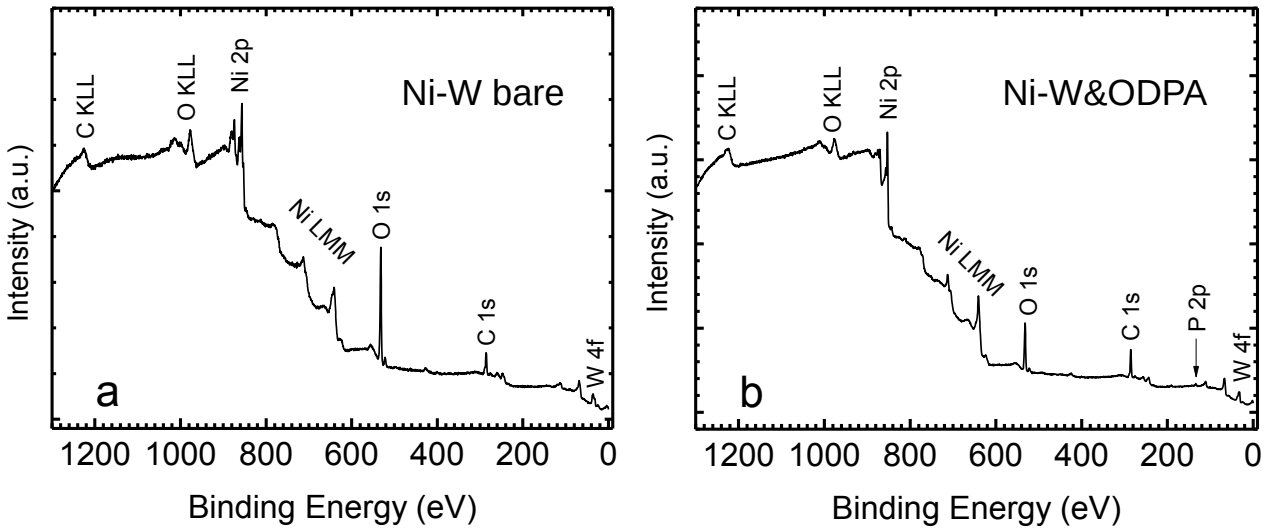

Figure 2*. Survey XPS spectra for Ni-W coatings (a) without functionalization and (b) with ODPA.*

The high resolution spectra (Figure 3b) in the P 2p region of sonicated Ni-W&ODPA samples exhibit a doublet at 133.5 eV, as reported in previous work for ODPA and phosphate monolayers on oxidized surfaces. [30, 32, 68] This result confirms the success of the functionalization procedure since bare Ni-W samples do not show any signal in the P 2p region (Figure 3a).

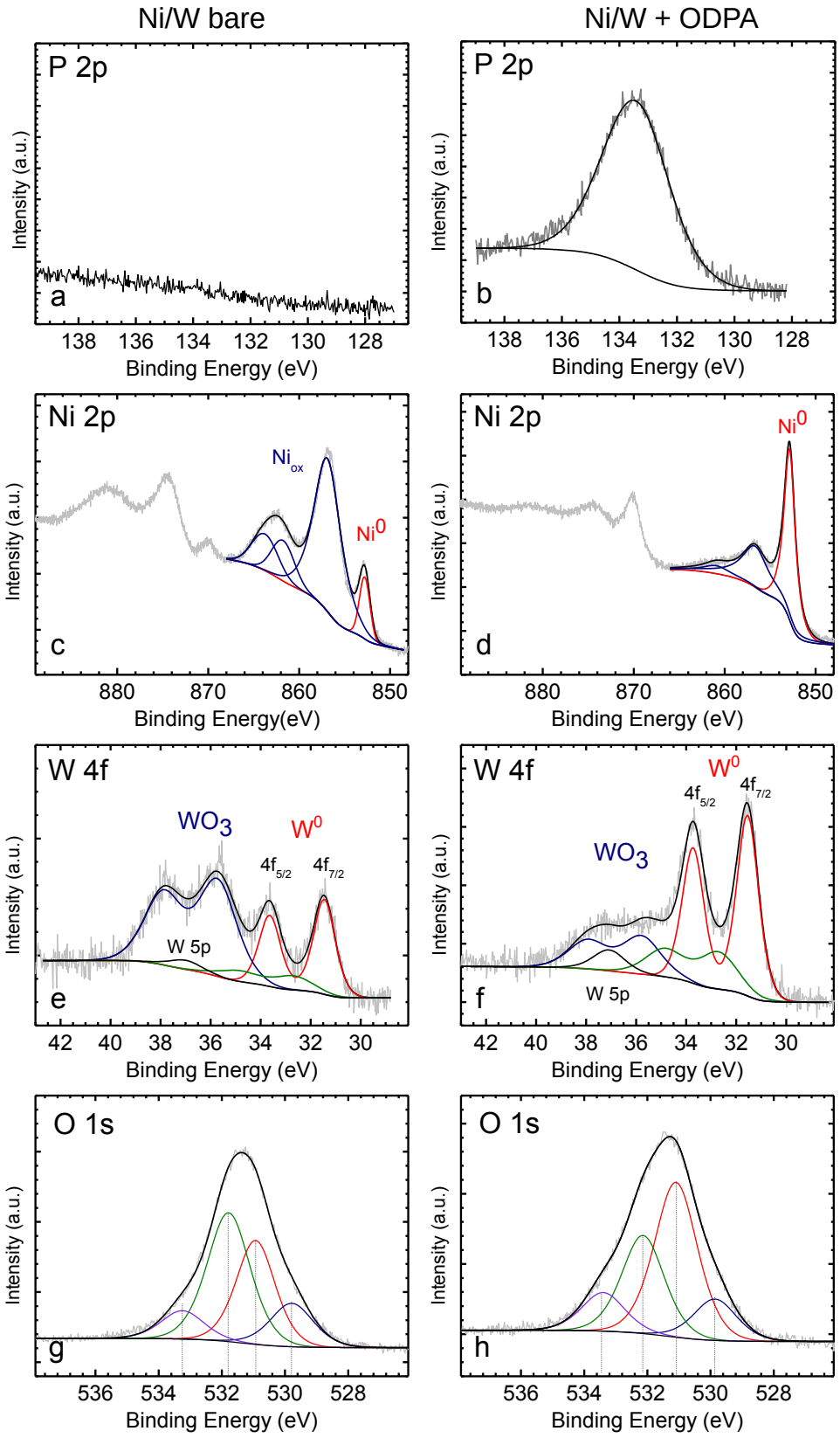

Figure 3. *XPS spectra for bare Ni-W coatings without functionalization (left side) and with ODPA (right side). (a-b) P 2p, (c-d) Ni 2p, (e-f) W 4f, (g-h) O 1s.*

On the other hand, in the Ni 2p and W 4f regions the high resolution spectra for bare Ni-W coatings exhibit the presence of both elements in their metallic state and their corresponding oxides: NiO, and NiOOH for Ni (Figure 3c); and WO_3 for W (Figure 3e). It has also been shown that after Ar^+ etching WO_3 was found deeper than the Ni oxides, but at ≈5 nm from the surface the WO_3 signal disappears.[6] More importantly, as revealed by Figure 3d and there is a marked decrease in the amount of oxides in Ni-W&ODPA with respect to the nonfunctionalized samples (Figure 3c and e). The decrease in the metal oxide/metal signal ratio suggests that the complex Ni and W oxide layer is thinner and partially replaced by the phosphonate layer. The O 1s (Figure 3g and h) analysis shed more light on the functionalization process. The component at 529.8 eV includes NiO and WO_3 , while that at 531 eV can be assigned to Ni hydroxide. After functionalization, the H_2O component at 532 eV clearly decreases while the component at 533.4 eV increases. This component is assigned to organic C=O (citrate) in the bare Ni/W surface, and in the functionalized sample it increases due to the oxygen incorporated by the ODPA molecules.[43] Thus, the decrease in the oxide signals with respect to the metal substrate in the ODPA functionalized sample (Figure 3 d and f) can be related to a thinner oxide layer resulting from both a reduction in the amount of water in the film due to the heat treatment at 100 C° and certain oxide dissolution during the condensation reaction of the Ni-W surface oxides with the phosphonic group leading to metal-O-P bonds. In fact, the thermal treatment transforms the weakly bonded phosphonic acid (hydrogen bonding [52] or ionic interactions [65]) layer into a phosphonate one driving away water molecules. Thus, the ODPA layer is strongly chemically bonded to the substrate by monodentate or mixed mono/bi/tri-dentate phosphonic heads.[43, 69] As can be seen in Figure 3h, the oxygen signal from Ni and W oxides (529.8 eV) is still present after functionalization, i.e. the oxide layer is not completely removed. Morover, the total O/P

atomic ratio is about 10, much higher than that expected for stoichometric Ni or W phosphonates.The covalent attachment to form P-O-Me bonds is demostrated by comparing the P spectra with that obtained for pure ODPA (Figure 4). The energy shift towards lower binding energies (from 134.3 eV to 133.5 eV) is indicative of the formation of a P-O-Metal bond in the Ni-W&ODPA samples. It will further be demonstrated that the compound improves the surface properties of the nanostructured alloy such as hydrophobicity and corrosion resistance.

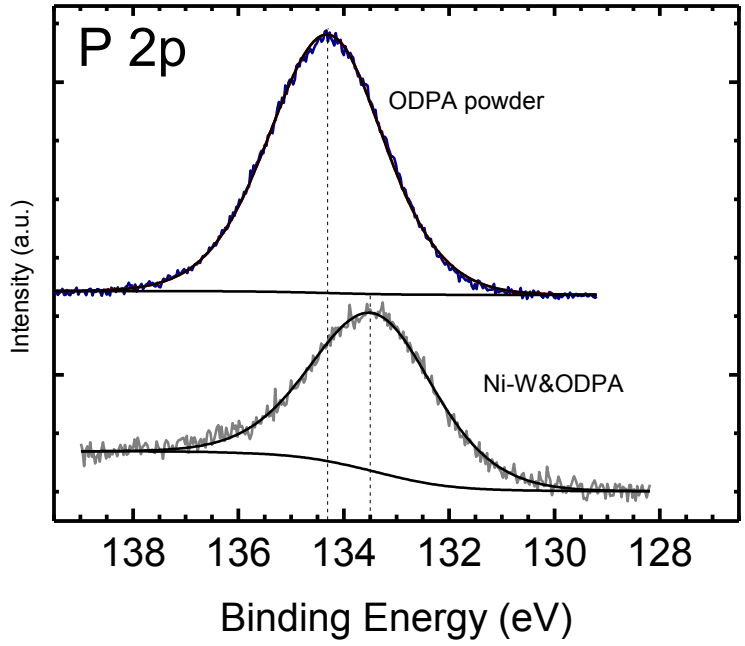

Figure 4. XPS P 2p spectra of pure solid ODPA (upper) and ODPA layer (lower) on Ni-W coating. Both spectra were charge corrected with C 1s peak at 285 eV. The energy shift towards lower binding energies (from 134.3 eV to 133.5 eV) is indicative of the formation of a P-O-Metal bond in the Ni-W&ODPA samples.

The static water contact angle for bare Ni–W increases from $\gamma = 73° \pm 4$ to $\gamma = 114° \pm 3$ after the ODPA treatment and sonication procedure. This result suggests that the organic layer turns the Ni-W surface highly hydrophobic. (Figure 5). After mechanical peel tests, the typical contact angles of the Ni-W&ODPA surfaces remained unaltered.

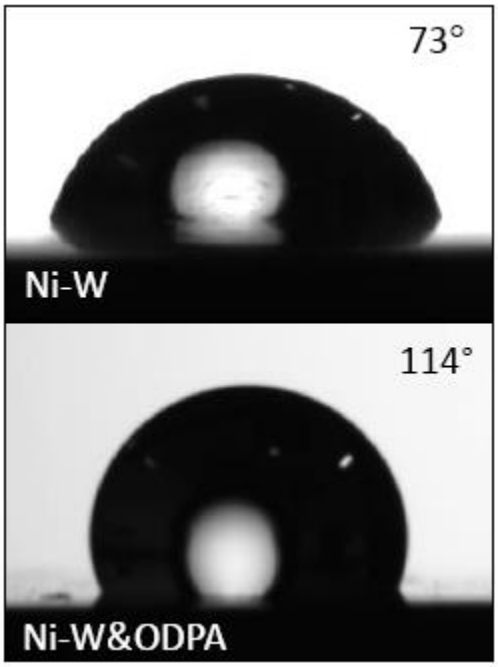

Figure 5. *Static water contact angle measurements of bare Ni–W surfaces before and after functionalization with ODPA.*

However, nano- and microscale roughness has been shown to affect the wettability but, in our samples, the morphology of the surfaces does not change after functionalization, as can be observed by AFM imaging. In fact, representative 10 μm in size images (Figure 6) taken at different regions of Ni-W surfaces before and after functionalization exhibit the same nanocrystalline structure with surface oxide grain sizes in the range 60-100 nm and, on average, the same root mean square roughness with typical rms values in the 40-45 nm range. Thus, the increase in contact angle should be assigned to the hydrophobic ODPA layer that conformally covers the underlying Ni-W surface without changing the nanoscale roughness of the functionalized sample. It should be noted that the phosphonate layer becomes more efficient than that obtained by Ni-W functionalization with tetraethoxysilane (TEOS) which exhibits $\gamma = 90°$. [18] In this case the TEOS layer needs to be improved by an additional step adding octadecyltrichlorosilane to obtain a contact angle ($\gamma = 119°$)[18] similar to that found on the Ni-

W&ODPA surface. The value $\gamma = 114^{\circ}$ is similar to those measured for phosphonate coatings on stainless steel ($\gamma = 108^{\circ}$), Nitiol ($\gamma = 107$), nickel ($\gamma = 109^{\circ}$) and titanium ($\gamma = 96^{\circ}$).[53]

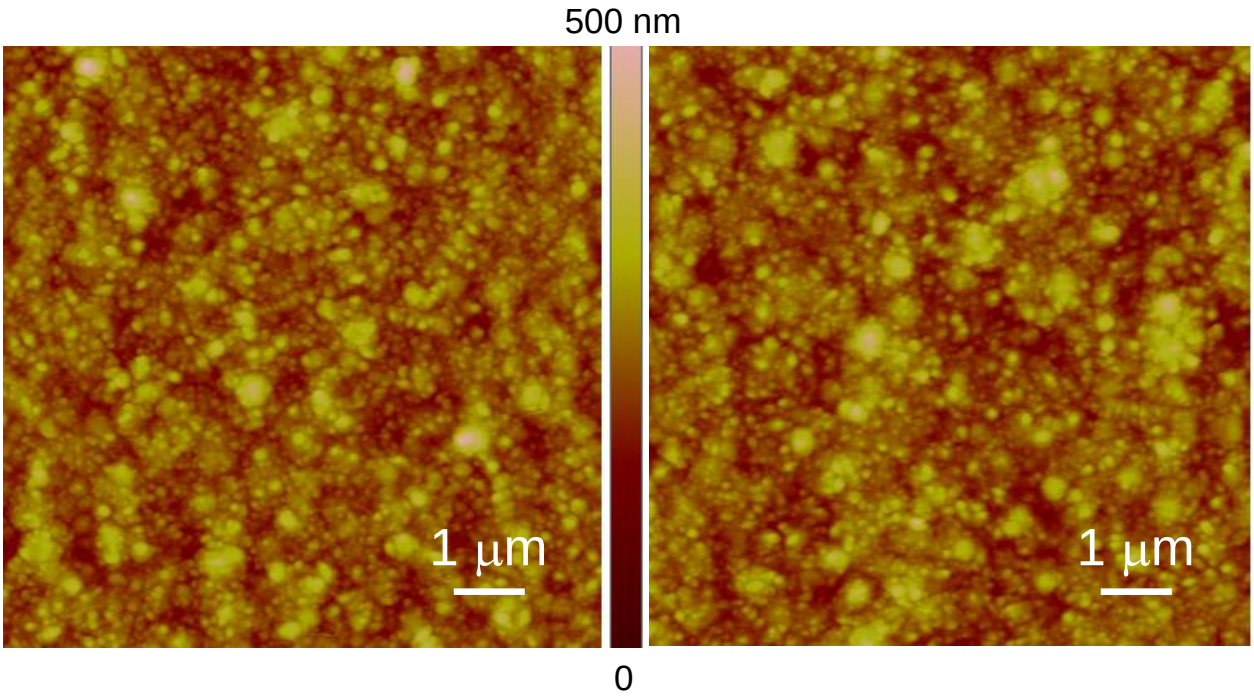

Figure 6. *Topographic 10μmx10μm AFM images for bare Ni-W (a) and Ni-W&ODPA samples(b) with no morphological changes after the functionalization. The color bar represents the z-scale.*

Finally, microhardness measurements on the cross-sections of the Ni-W&ODPA samples result in ≈ 650-750 HV values, i.e. the ODPA treatment does not change the typical value reported for this alloy. [6, 10] Microhardness measurements made on the surface of the samples exhibit the same values for Ni-W and Ni-W&ODPA. These results confirm that the functionalization procedure does not alter the mechanical properties of the coatings.

The electrochemical behavior of Ni-W&ODPA samples gives crucial information about the effectiveness of the functionalization procedure to protect the surfaces against corrosion aqueous media containing chloride ions.

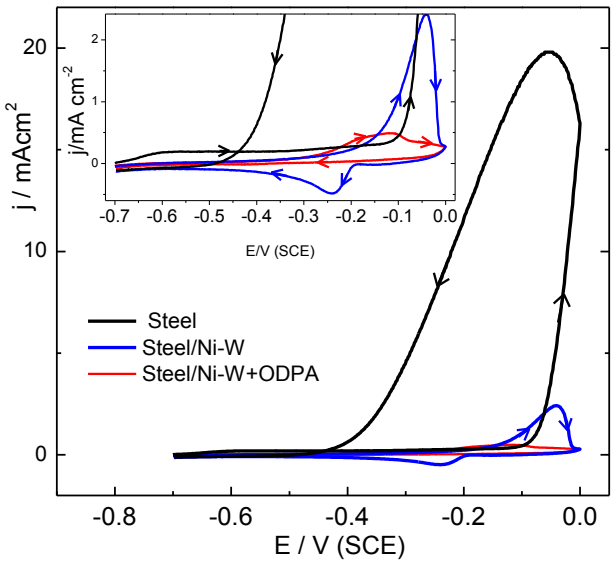

Figure 7. *Cyclic voltammograms at v = 0.020 V $s^{-1}$of steel (black), Ni-W electrodeposited on steel (blue) and Ni-W&ODPA (red) samples in a still deaerated phosphate–borate buffer (0.1 M KH_2PO_4 + 0.05 M $Na_2B_4O_7$) pH 8.00, with the addition of 0.5 M NaCl to the same solution. The inset is a magnification of the current scale to show the differences in corrosion behavior.*

First, we will explore the anodic behavior of the different samples by cyclic voltammetry in the -0.7 V < E < 0.0 V potential range (Figure 7). Thus, in the anodic excursion (Figure 7, black line inset) the steel samples exhibit the oxide formation at -0.6 V followed by a current plateau corresponding to the passive region (Figure 7 inset), and finally at E > -0.10 V, a sudden increase in current associated with passivity breakdown induced by the aggressive Cl^- anions and subsequent pitting corrosion. The repassivation potential for the pits is located at about -0.42 V. For Ni-W and Ni-W&ODPA coated steel samples the behavior is totally different in the same potential range discussed previously for the bare steel. No pitting processes are visible, and the typical behavior of the formation of passive oxides is observed in the -0.30- 0 V potential region (blue and red curves in Figure 7 and inset). For Ni-W surfaces the amount of charge involved in the anodic peak (blue line in Figure 7 and inset) is higher than in the cathodic scan indicating that, in addition to oxide formation, some corrosion of the alloy through the oxide layer takes

place during the anodic process. A similar behavior is observed for ODPA functionalized samples (red line in Figure 7 and inset), although the current density in the overall potential range is smaller than that recorded for the bare alloy. The morphology of Ni-W and Ni-W&ODPA surfaces after an anodic excursion up to 0 V run at at 0.020 V s^{-1} in still deaerated phosphate–borate buffer (0.1 M KH_2PO_4 + 0.05 M $Na_2B_4O_7$) pH 8.00, with the addition of 0.5 M NaCl to the same solution show the absence of pits as it is observed in the steel sample (Figure S1.a and b). Although some regions of Ni-W seems to indicate the initial stages of localized corrosion (Figure S1.c) the exploration of many regions of that surface with AFM microscopy (images not shown) does not reveal that they have the typical morphology of the pits observed for steel (Figure S1.b). Ni-W&ODPA surfaces do not exhibit localized corrosion (Figure S1.d). These result confirm the hydrophobic nature of the organic layer that hinders the transport of water from the solution to the alloy surface needed for oxide formation, as well as the transport of metal ions resulting from the dissolution process from the metal surface to the solution side. Chloride anions of the solution are also impeded to reach the alloy surface through the hydrophobic ODPA layer.

However, in order to predict the corrosion behavior of steel with the different coatings, slow potentiodynamic curves are needed in both the cathodic and anodic potential regions. This is particularly important for pitting corrosion as the potential associated with pitting initiation could involve significant induction times. In Figure 8 we present cathodic (Figure 8a) and anodic (Figure 8b) current vs potential curves for the steel samples recorded at 0.002 V s^{-1} in deaerated NaCl containing solutions. The cathodic curves recorded for the Ni-W&ODPA samples exhibit a marked decrease in the current associated with the hydrogen evolution reaction in relation to the steel and Ni-W samples, thus reflecting the hindered water transport across the organic layer (Figure 8a). Also, the anodic behavior is markedly different. Steel samples exhibit a plateau with

very small currents in the -0.66 V/-0.20 V region, which at this scan rate is mainly associated with alloy dissolution through the passive oxide layer, followed by an abrupt increase in current at E > -0.20 V due to passivity breakdown and pitting corrosion of the steel. The anodic curve for the Ni-W coated steel at this slow scan rate also reveals signs of pit initiation at E > -0.1 V. In contrast, no pitting is observed for Ni-W&ODPA coated steel samples in this potential range, i.e., the transport of the Cl^- ions needed for passivity breakdown is largely impeded for the ODPA layer.

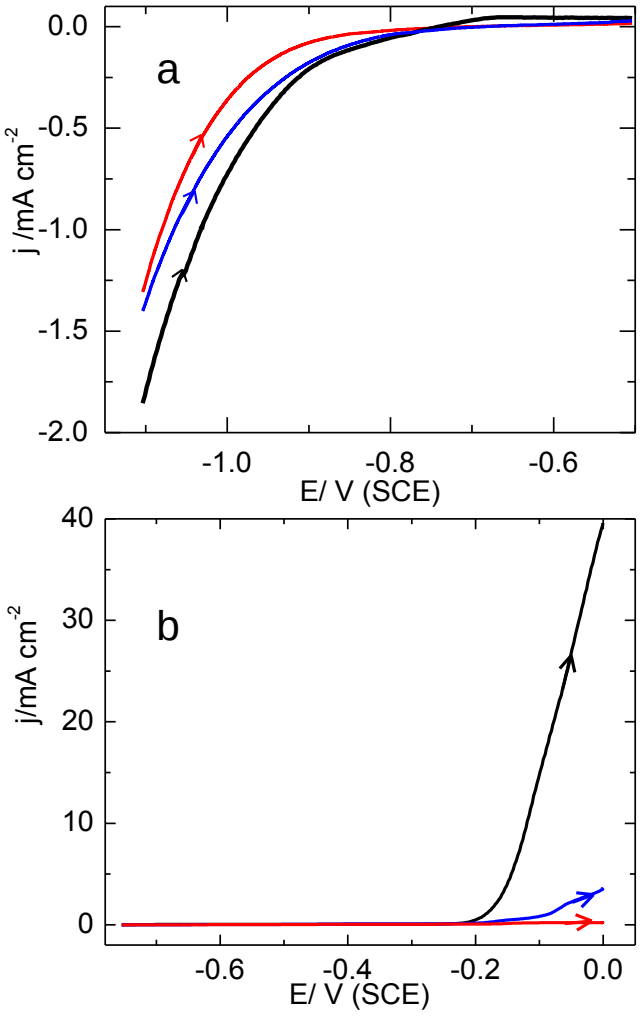

***Figure 8**. Potentiodynamic polarization curves at low scan rate (v= 0.002 V s^{-1}) for steel (black), Ni-W (blue) and Ni-W&ODPA (red) samples in a still deaerated phosphate–borate buffer (0.1 M KH_2PO_4 + 0.05 M $Na_2B_4O_7$) pH 8.00, with the addition of 0.5 M NaCl into the same solution. (a) -1.1/-0.5 V range (b) -0.5/0 V range.*

Impedance spectroscopy was used to compare the behavior for the three surfaces in chloride-containing solutions at open circuit potential (OCP). Figure 9 shows the EIS data for the three surfaces. The Nyquist plot of steel shows a capacitive loop at high and intermediate frequencies and a not well-defined contribution al lower frequencies. The Nyquist plots of Ni-W and Ni-W&ODPA samples exhibit a single well-defined semicircle covering the whole range of frequencies. These results can be interpreted in terms of the following general total transfer function:

$Z_T(j\omega) = R_\Omega + Z(j\omega)$

where $Z_T(j\omega)$ is the total impedance, R_Ω is the electrolyte resistance contribution, $\omega = 2\pi f$, f is the frequency, and $Z(j\omega)$ is the impedance of the interface that is specific to the electrochemical system.

The impedance of the interface $Z(j\omega)$ is:

$[Z(j\omega)]^{-1} = [Z_{CPE}]^{-1} + [Rct]^{-1}$

where $Z_{CPE} = [C_{dl}(j\omega)^{\alpha}]^{-1}$ is the constant phase element; C_{dl} is the double-layer capacitance, the exponent α accounts for the distribution of the time constants due to the surface inhomogeneities, and Rct is the charge transfer resistance. The good agreement between the experimental and fitted data was checked thorough Bode plots (data not shown) The high R_{ct} (~ 35000 ohm cm^{-2}) and α values (0.92) of Ni-W&ODPA samples with respect to Ni-W (R_{ct} ~ 7900 ohm cm^{-2}), α (0.88) and steel (R_{ct} ~ 690 ohm cm^{-2}), α (0.79) confirm that ODPA provides a protective uniform layer to Ni-W coatings.

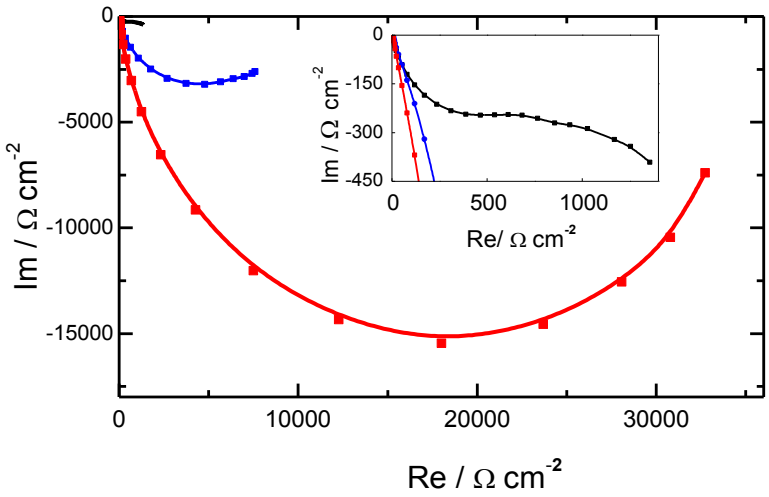

Figure 9. Nyquist plots for steel (black), Ni-W (blue) and Ni-W&ODPA (red). The inset is a magnification in the high frequency range. EIS data were taken at OCP in still deaerated phosphate–borate buffer (0.1 M KH_2PO_4 + 0.05 M $Na_2B_4O_7$) pH 8.00, with the addition of 0.5 M NaCl to the same solution.

The present results demonstrate that ODPA can be used as an efficient protective coating for Ni-W alloys. Taking into account the complex chemical nature of the surface oxides composed of a mixture of W and Ni oxides and hydroxides, one could wonder about the role of these species in the formation and stability of the ODPA layer. According to the theory, the pKa of the organic acid has to be lower than the isoelectric point of the metal oxide (IEP) to be capable of forming ordered films on the metal oxide surfaces. [53] In this context, higher IEP give rise to more reactive surfaces towards the acid favoring stronger coordination bonds. In our system the pKa of the phosphonic acid (4.5) [70] is lower than the IEP of nickel oxides/hydroxides (≈11), but it is larger than the IEP of W oxides/hydroxides (≈2.8). [71] Therefore, the nickel oxide/hydroxide seems to have a key role in the formation of the stable ODPA layer.

Conclusions

We have shown that phosphonates are able to self-assemble on Ni-W coated steel improving its surface properties in terms of hydrophobicity and corrosion resistance. The organic layer survives washing and sonication procedures, and electrochemical measurements in a wide

potential range, indicating that it is strongly bonded to the surface oxides. The analysis of the phosphonate stability in terms of the pKa of the phosphonic acid and the isoelectric points of the metallic oxides suggests that the nickel oxides have a key role in ODPA formation and stabilization.

Acknowledgments

We acknowledge financial support from ANPCyT (PICT 2012-1808), CONICET (PIP 0671) and Universidad Nacional de La Plata (11X760). MEV is member of the research career of CICPBA. The authors wish to thank Eng. Carlos Llorente and Adriana Barboza (LIMF, Facultad de Ingeniería, Universidad Nacional de La Plata, Argentina) for carrying out microhardness determinations.

References

[1] T. Yamasaki, P. Schloβmacher, K. Ehrlich, Y. Ogino, Formation of amorphous electrodeposited Ni-W alloys and their nanocrystallization, Nanostruct. Mater. 10 (1998) 375-388.

[2] T. Yamasaki, High-strength nanocrystalline Ni-W alloys produced by electrodeposition, Mater. Phys. Mech. 1 (2000) 127-132.

[3] C.A. Schuh, T.G. Nieh, H. Iwasaki, The effect of solid solution W additions on the mechanical properties of nanocrystalline Ni, Acta Mater. 51 (2003) 431-443.

[4] N. Eliaz, T.M. Sridhar, E. Gileadi, Synthesis and characterization of nickel tungsten alloys by electrodeposition, Electrochim. Acta 50 (2005) 2893-2904.

[5] P. de Lima-Neto, A.N. Correia, R.A.C. Santana, R.P. Colares, E.B. Barros, P.N.S. Casciano, G.L. Vaz, Morphological, structural, microhardness and electrochemical characterisations of electrodeposited Cr and Ni–W coatings, Electrochim. Acta 55 (2010) 2078-2086.

[6] M.P. Quiroga Argañaraz, S.B. Ribotta, M.E. Folquer, L.M. Gassa, G. Benítez, M.E. Vela, R.C. Salvarezza, Ni–W coatings electrodeposited on carbon steel: Chemical composition, mechanical properties and corrosion resistance, Electrochim. Acta 56 (2011) 5898-5903.

[7] A. Chianpairot, G. Lothongkum, C.A. Schuh, Y. Boonyongmaneerat, Corrosion of nanocrystalline Ni–W alloys in alkaline and acidic 3.5wt.% NaCl solutions, Corros. Sci. 53 (2011) 1066-1071.

[8] M.A. Farzaneh, M.R. Zamanzad-Ghavidel, K. Raeissi, M.A. Golozar, A. Saatchi, S. Kabi, Effects of Co and W alloying elements on the electrodeposition aspects and properties of nanocrystalline Ni alloy coatings, Appl. Surf. Sci. 257 (2011) 5919-5926.

[9] C. Borgia, T. Scharowsky, A. Furrer, C. Solenthaler, R. Spolenak, A combinatorial study on the influence of elemental composition and heat treatment on the phase composition, microstructure and mechanical properties of Ni–W alloy thin films, Acta Mater. 59 (2011) 386-399.

[10] M.P. Quiroga Argañaraz, S.B. Ribotta, M.E. Folquer, E. Zelaya, C. Llorente, J.M. Ramallo-López, G. Benítez, A. Rubert, L.M. Gassa, M.E. Vela, R.C. Salvarezza, The chemistry and structure of nickel-tungsten coatings obtained by pulse galvanostatic electrodeposition, Electrochim. Acta 72 (2012) 87-93.
[11] W. Sassi, L. Dhouibi, P. Berçot, M. Rezrazi, E. Triki, Effect of pyridine on the electrocrystallization and corrosion behavior of Ni–W alloy coated from citrate–ammonia media, Appl. Surf. Sci. 263 (2012) 373-381.
[12] Y. Sui, C. Sun, J. Sun, B. Pu, W. Ren, W. Zhao, Stability of an Electrodeposited Nanocrystalline Ni-Based Alloy Coating in Oil and Gas Wells with the Coexistence of H2S and CO2, Materials 10 (2017).
[13] J. Sagiv, Organized monolayers by adsorption. 1. Formation and structure of oleophobic mixed monolayers on solid surfaces, J. Am. Chem. Soc. 102 (1980) 92-98.
[14] A. Ulman, An Introduction to Ultrathin Organic Films: From Langmuir-Blodgett to Self-Assembly, Academic Press, Boston, 1991.
[15] C. Queffélec, M. Petit, P. Janvier, D.A. Knight, B. Bujoli, Surface Modification Using Phosphonic Acids and Esters, Chem. Rev. 112 (2012) 3777-3807.
[16] B.M. Silverman, K.A. Wieghaus, J. Schwartz, Comparative Properties of Siloxane vs Phosphonate Monolayers on A Key Titanium Alloy, Langmuir 21 (2005) 225-228.
[17] S.H. Zaferani, M. Peikari, D. Zaarei, I. Danaee, J.M. Fakhraei, M. Mohammadi, Using Silane Films to Produce an Alternative for Chromate Conversion Coatings, Corrosion 69 (2013) 372-387.
[18] M.P. Quiroga Arganaraz, J.M. Ramallo-Lopez, G. Benitez, A. Rubert, E.D. Prieto, L.M. Gassa, R.C. Salvarezza, M.E. Vela, Optimization of the surface properties of nanostructured Ni-W alloys on steel by a mixed silane layer, PCCP 17 (2015) 14201-14207.
[19] R.-G. Hu, S. Zhang, J.-F. Bu, C.-J. Lin, G.-L. Song, Recent progress in corrosion protection of magnesium alloys by organic coatings, Prog. Org. Coat. 73 (2012) 129-141.
[20] K.J. Gagnon, H.P. Perry, A. Clearfield, Conventional and Unconventional Metal–Organic Frameworks Based on Phosphonate Ligands: MOFs and UMOFs, Chem. Rev. 112 (2012) 1034-1054.
[21] G. Hähner, R. Hofer, I. Klingenfuss, Order and Orientation in Self-Assembled Long Chain Alkanephosphate Monolayers Adsorbed on Metal Oxide Surfaces, Langmuir 17 (2001) 7047-7052.
[22] I.L. Liakos, R.C. Newman, E. McAlpine, M.R. Alexander, Comparative study of self-assembly of a range of monofunctional aliphatic molecules on magnetron-sputtered aluminium, Surf. Interface Anal. 36 (2004) 347-354.
[23] E. Hoque, J.A. DeRose, P. Hoffmann, H.J. Mathieu, B. Bhushan, M. Cichomski, Phosphonate self-assembled monolayers on aluminum surfaces, J.Chem.Phys. 124 (2006) 174710.
[24] I. Levine, S.M. Weber, Y. Feldman, T. Bendikov, H. Cohen, D. Cahen, A. Vilan, Molecular Length, Monolayer Density, and Charge Transport: Lessons from Al–AlOx/Alkyl–Phosphonate/Hg Junctions, Langmuir 28 (2012) 404-415.
[25] D. Chen, H.K. Yin Wu, S. Naderi-Gohar, Y. Wu, Y. Huang, H.-Y. Nie, An extremely rapid dip-coating method for self-assembly of octadecylphosphonic acid and its thermal stability on an aluminum film, J.Mater.Chem.C 2 (2014) 9941-9948.

[26] A. Debrassi, E. Roeven, S. Thijssen, L. Scheres, W.M. de Vos, T. Wennekes, H. Zuilhof, Versatile (Bio)Functionalization of Bromo-Terminated Phosphonate-Modified Porous Aluminum Oxide, Langmuir 31 (2015) 5633-5644.
[27] H. Ma, O. Acton, D.O. Hutchins, N. Cernetic, A.K.Y. Jen, Multifunctional phosphonic acid self-assembled monolayers on metal oxides as dielectrics, interface modification layers and semiconductors for low-voltage high-performance organic field-effect transistors, PCCP 14 (2012) 14110-14126.
[28] O. Yildirim, M.D. Yilmaz, D.N. Reinhoudt, D.H.A. Blank, G. Rijnders, J. Huskens, Electrochemical Stability of Self-Assembled Alkylphosphate Monolayers on Conducting Metal Oxides, Langmuir 27 (2011) 9890-9894.
[29] E.S. Gawalt, M.J. Avaltroni, N. Koch, J. Schwartz, Self-Assembly and Bonding of Alkanephosphonic Acids on the Native Oxide Surface of Titanium, Langmuir 17 (2001) 5736-5738.
[30] D.M. Spori, N.V. Venkataraman, S.G.P. Tosatti, F. Durmaz, N.D. Spencer, S. Zürcher, Influence of Alkyl Chain Length on Phosphate Self-Assembled Monolayers, Langmuir 23 (2007) 8053-8060.
[31] S. Clair, F. Variola, M. Kondratenko, P. Jedrzejowski, A. Nanci, F. Rosei, D.F. Perepichka, Self-assembled monolayer of alkanephosphoric acid on nanotextured Ti, J.Chem.Phys. 128 (2008) 144705.
[32] N. Metoki, L. Liu, E. Beilis, N. Eliaz, D. Mandler, Preparation and Characterization of Alkylphosphonic Acid Self-Assembled Monolayers on Titanium Alloy by Chemisorption and Electrochemical Deposition, Langmuir 30 (2014) 6791-6799.
[33] D.L. Ashford, A.M. Lapides, A.K. Vannucci, K. Hanson, D.A. Torelli, D.P. Harrison, J.L. Templeton, T.J. Meyer, Water Oxidation by an Electropolymerized Catalyst on Derivatized Mesoporous Metal Oxide Electrodes, J. Am. Chem. Soc. 136 (2014) 6578-6581.
[34] K. Rudzka, A.Y. Sanchez Treviño, M.A. Rodríguez-Valverde, M.A. Cabrerizo-Vílchez, Formation of mixed and patterned self-assembled films of alkylphosphonates on commercially pure titanium surfaces, Appl. Surf. Sci. 389 (2016) 270-277.
[35] A. Forget, B. Limoges, V. Balland, Efficient Chemisorption of Organophosphorous Redox Probes on Indium Tin Oxide Surfaces under Mild Conditions, Langmuir 31 (2015) 1931-1940.
[36] L. Sang, K.M. Knesting, A. Bulusu, A.K. Sigdel, A.J. Giordano, S.R. Marder, J.J. Berry, S. Graham, D.S. Ginger, J.E. Pemberton, Effect of time and deposition method on quality of phosphonic acid modifier self-assembled monolayers on indium zinc oxide, Appl. Surf. Sci. 389 (2016) 190-198.
[37] X. Wang, M. Lieberman, Zirconium−Phosphonate Monolayers with Embedded Disulfide Bonds, Langmuir 19 (2003) 7346-7353.
[38] R.M. Fabre, D.R. Talham, Stable Supported Lipid Bilayers on Zirconium Phosphonate Surfaces, Langmuir 25 (2009) 12644-12652.
[39] M. Textor, L. Ruiz, R. Hofer, A. Rossi, K. Feldman, G. Hähner, N.D. Spencer, Structural Chemistry of Self-Assembled Monolayers of Octadecylphosphoric Acid on Tantalum Oxide Surfaces, Langmuir 16 (2000) 3257-3271.
[40] T. Ishizaki, M. Okido, Y. Masuda, N. Saito, M. Sakamoto, Corrosion Resistant Performances of Alkanoic and Phosphonic Acids Derived Self-Assembled Monolayers on Magnesium Alloy AZ31 by Vapor-Phase Method, Langmuir 27 (2011) 6009-6017.

[41] S. Szillies, P. Thissen, D. Tabatabai, F. Feil, W. Fürbeth, N. Fink, G. Grundmeier, Formation and stability of organic acid monolayers on magnesium alloy AZ31: The role of alkyl chain length and head group chemistry, Appl. Surf. Sci. 283 (2013) 339-347.
[42] R. Adadi, G. Zorn, R. Brener, I. Gotman, E.Y. Gutmanas, C.N. Sukenik, Phosphonate-anchored thin films on titanium and niobium oxide surfaces: Fabrication and characterization, Thin Solid Films 518 (2010) 1966-1972.
[43] I. Gouzman, M. Dubey, M.D. Carolus, J. Schwartz, S.L. Bernasek, Monolayer vs. multilayer self-assembled alkylphosphonate films: X-ray photoelectron spectroscopy studies, Surf. Sci. 600 (2006) 773-781.
[44] G. Zorn, R. Adadi, R. Brener, V.A. Yakovlev, I. Gotman, E.Y. Gutmanas, C.N. Sukenik, Tailoring the Surface of NiTi Alloy Using PIRAC Nitriding Followed by Anodization and Phosphonate Monolayer Deposition, Chem. Mater. 20 (2008) 5368-5374.
[45] R. Quiñones, E.S. Gawalt, Study of the formation of self-assembled monolayers on nitinol, Langmuir 23 (2007) 10123-10130.
[46] G. Fonder, I. Minet, C. Volcke, S. Devillers, J. Delhalle, Z. Mekhalif, Anchoring of alkylphosphonic derivatives molecules on copper oxide surfaces, Appl. Surf. Sci. 257 (2011) 6300-6307.
[47] K.M. Kruszewski, E.R. Renk, E.S. Gawalt, Self-assembly of organic acid molecules on the metal oxide surface of a cupronickel alloy, Thin Solid Films 520 (2012) 4326-4331.
[48] R. Bhure, T.M. Abdel-Fattah, C. Bonner, F. Hall, A. Mahapatro, Stability of Phosphonic Self Assembled Monolayers (SAMs) on Cobalt Chromium (Co-Cr) Alloy under Oxidative conditions, Appl. Surf. Sci. 257 (2011) 5605-5612.
[49] J. Rechmann, A. Sarfraz, A.C. Götzinger, E. Dirksen, T.J.J. Müller, A. Erbe, Surface Functionalization of Oxide-Covered Zinc and Iron with Phosphonated Phenylethynyl Phenothiazine, Langmuir 31 (2015) 7306-7316.
[50] A. Raman, M. Dubey, I. Gouzman, E.S. Gawalt, Formation of Self-Assembled Monolayers of Alkylphosphonic Acid on the Native Oxide Surface of SS316L, Langmuir 22 (2006) 6469-6472.
[51] J.W. Chan, A. Huang, K.E. Uhrich, Self-Assembled Amphiphilic Macromolecule Coatings: Comparison of Grafting-From and Grafting-To Approaches for Bioactive Delivery, Langmuir 32 (2016) 5038-5047.
[52] M.S. Lim, K.J. Smiley, E.S. Gawalt, Thermally driven stability of octadecylphosphonic acid thin films grown on SS316L, Scanning 32 (2010) 304-311.
[53] A. Raman, R. Quiñones, L. Barriger, R. Eastman, A. Parsi, E.S. Gawalt, Understanding Organic Film Behavior on Alloy and Metal Oxides, Langmuir 26 (2010) 1747-1754.
[54] M. Alonso Frank, C. Meltzer, B. Braunschweig, W. Peukert, A.R. Boccaccini, S. Virtanen, Functionalization of steel surfaces with organic acids: Influence on wetting and corrosion behavior, Appl. Surf. Sci. 404 (2017) 326-333.
[55] M. Dubey, T. Weidner, L.J. Gamble, D.G. Castner, Structure and Order of Phosphonic Acid-Based Self-Assembled Monolayers on Si(100), Langmuir 26 (2010) 14747-14754.
[56] A. Cattani-Scholz, K.-C. Liao, A. Bora, A. Pathak, C. Hundschell, B. Nickel, J. Schwartz, G. Abstreiter, M. Tornow, Molecular Architecture: Construction of Self-Assembled Organophosphonate Duplexes and Their Electrochemical Characterization, Langmuir 28 (2012) 7889-7896.
[57] H. Benbenishty-Shamir, R. Gilert, I. Gotman, E.Y. Gutmanas, C.N. Sukenik, Phosphonate-Anchored Monolayers for Antibody Binding to Magnetic Nanoparticles, Langmuir 27 (2011) 12082-12089.

[58] D.M. Rampulla, C.M. Wroge, E.L. Hanson, J.G. Kushmerick, Charge Transport across Phosphonate Monolayers on Indium Tin Oxide, J.Phys.Chem.C 114 (2010) 20852-20855.
[59] S.P. Pujari, L. Scheres, A.T.M. Marcelis, H. Zuilhof, Covalent Surface Modification of Oxide Surfaces, Angew. Chem. Int. Ed. 53 (2014) 6322-6356.
[60] R.N. Jones, R.A. Ripley, The Raman Spectra of Deuterated Methyl Laurates and Related Compounds, Can. J. Chem. 42 (1964) 305-325.
[61] A.N. Parikh, M.A. Schivley, E. Koo, K. Seshadri, D. Aurentz, K. Mueller, D.L. Allara, n-Alkylsiloxanes: From Single Monolayers to Layered Crystals. The Formation of Crystalline Polymers from the Hydrolysis of n-Octadecyltrichlorosilane, J. Am. Chem. Soc. 119 (1997) 3135-3143.
[62] E. Podstawka, A. Kudelski, T.K. Olszewski, B. Boduszek, Surface-Enhanced Raman Scattering Studies on the Interaction of Phosphonate Derivatives of Imidazole, Thiazole, and Pyridine with a Silver Electrode in Aqueous Solution, J.Phys.Chem.B 113 (2009) 10035-10042.
[63] N.L. Jeon, K. Finnie, K. Branshaw, R.G. Nuzzo, Structure and Stability of Patterned Self-Assembled Films of Octadecyltrichlorosilane Formed by Contact Printing, Langmuir 13 (1997) 3382-3391.
[64] R. Luschtinetz, G. Seifert, E. Jaehne, H.-J.P. Adler, Infrared Spectra of Alkylphosphonic Acid Bound to Aluminium Surfaces, Macromolecular Symposia 254 (2007) 248-253.
[65] P. Thissen, M. Valtiner, G. Grundmeier, Stability of Phosphonic Acid Self-Assembled Monolayers on Amorphous and Single-Crystalline Aluminum Oxide Surfaces in Aqueous Solution, Langmuir 26 (2010) 156-164.
[66] Y. Yu, K. Lin, X. Zhou, H. Wang, S. Liu, X. Ma, New C−H Stretching Vibrational Spectral Features in the Raman Spectra of Gaseous and Liquid Ethanol, J.Phys.Chem.C 111 (2007) 8971-8978.
[67] R. Juškėnas, I. Valsiūnas, V. Pakštas, R. Giraitis, On the state of W in electrodeposited Ni–W alloys, Electrochim. Acta 54 (2009) 2616-2620.
[68] C.E.B. Marino, P.A.P. Nascente, S.R. Biaggio, R.C. Rocha-Filho, N. Bocchi, XPS characterization of anodic titanium oxide films grown in phosphate buffer solutions, Thin Solid Films 468 (2004) 109-112.
[69] I. Milošev, M. Metikoš-Huković, Ž. Petrović, Influence of preparation methods on the properties of self-assembled films of octadecylphosphonate on Nitinol: XPS and EIS studies, Mater. Sci. Eng., C 32 (2012) 2604-2616.
[70] D.A. Smith, M.L. Wallwork, J. Zhang, J. Kirkham, C. Robinson, A. Marsh, M. Wong, The Effect of Electrolyte Concentration on the Chemical Force Titration Behavior of ω-Functionalized SAMs: Evidence for the Formation of Strong Ionic Hydrogen Bonds, J.Phys.Chem.B 104 (2000) 8862-8870.
[71] M. Kosmulski, Compilation of PZC and IEP of sparingly soluble metal oxides and hydroxides from literature, Adv. Colloid Interface Sci. 152 (2009) 14-25.